Nat. Hazards Earth Syst. Sci. Discuss., 1, 1213–1256, 2013
www.nat-hazards-earth-syst-sci-discuss.net/1/1213/2013/
doi:10.5194/nhessd-1-1213-2013

Natural Hazards and Earth System Sciences
Discussions

Advanced interpretation of land subsidence by validating multi-interferometric SAR data: the case study of the Anthemountas basin (northern Greece)

F. Raspini[1], C. Loupasakis[2], D. Rozos[2], and S. Moretti[1]

[1]Department of Earth Sciences, University of Firenze, Firenze, Italy
[2]Laboratory of Engineering Geology and Hydrogeology, Department of Geological Sciences, School of Mining and Metallurgical Engineering, National Technical University of Athens, Athens, Greece

Received: 12 February 2013 – Accepted: 22 March 2013 – Published: 11 April 2013

Correspondence to: F. Raspini (federico.raspini@unifi.it)

Published by Copernicus Publications on behalf of the European Geosciences Union.

Abstract

The potential of repeat-pass space borne SAR (Synthetic Aperture Radar) interferometry has been exploited to investigate spatial patterns of land subsidence in the Anthemountas basin, in the northern part of Greece. The PSI (Persistent Scatterer Interferometry) approach, based on the processing of long series of SAR acquisitions, has been applied to forty-two images acquired in 1995–2001 by ERS1/2 satellites. Interferometric results have been analyzed at a basin scale as support for land motion mapping and at local scale for the characterization of ground motion events affecting the village of Perea in the Thermaikos municipality and the "Macedonia" international airport.

PSI results revealed a moderate subsidence phenomenon along the wider coastal zone of Anthemountas basin corresponding to intense groundwater extraction. Highest values, exceeding 20 mm yr^{-1}, were measured in the airport area where the thickest sequence of compressible Quaternary sediments occurs. Intense subsidence has been detected also in the Perea village (maximum deformation up to 10–15 mm yr^{-1}), where a series of fractures, causing damages to both buildings and infrastructure, occurred in 2005–2006. Furthermore, a linear pattern of deformation, elongated parallel to the major normal Thermi fault, has been observed, indicating movements with a probable tectonic component.

1 Introduction

Several regions in Greece experience land subsidence due to the overexploitation of the aquifers during the last decades. The Thessaly Plain (Kaplanides and Fountoulis, 1997; Kontogianni et al., 2007; Rozos et al., 2010), Kalochori village in the east sector of Thessaloniki plain (Andronopoulos et al., 1991; Stiros, 2001; Psimoulis et al., 2007; Raucoules et al., 2008; Loupasakis and Rozos, 2009 and references therein), the region extending at the west–southwest of the Anargyri opencast coalmine in west

Macedonia (Soulios et al., 2011), Megalopolis in Peloponnesus (Dimitrakopoulos and Koumantakis 1995) and the Messara valley in Crete (Mertikas and Papadaki, 2009) are some, of the well-known areas presenting ground subsidence, related to reservoir compaction, in Greece.

These land subsidence phenomena extend gently over large areas, present low deformation rates and take place for several decades, sometimes without being noticed at the beginning. Localized differential ground deformations can trigger damages on structures as well as loss of functionality of linear and point infrastructures (pipeline and road network deformations, well-casing failures and protrusion, etc.).

One of challenging aspects in dealing with analysis of subsidence phenomena is that their mechanism is not easily detectable. The overlapping of different sources of deformation complicates the interpretation of the phenomenon. In most of the cases land subsidence is complex, reflecting a combination of anthropogenic and natural causes. For instance, the natural compaction of unconsolidated fine-grained deposits may be accentuated by human activities, such as over-exploitation of groundwater resource. Moreover, neotectonic activity, spatial variability of geotechnical parameters, temporal variability of water extraction rate may contribute to the different deformation patterns throughout the affected areas.

Detecting, measuring and monitoring subsidence is fundamental for hazard zonation and risk management. Analysis and research on deformation mechanisms are usually limited by the lack of data concerning the rate, spatial extent and temporal evolution of subsidence. Distribution of deformation can be assessed by using purely conventional, ground-based geodetic instruments, such as leveling (e.g. Phien-wej et al., 2006) and GPS (e.g. Ikehara, 1994) or exploiting new remotely sensed methods (e.g. Galloway and Hoffman, 2007; Galloway and Burbey, 2011).

The current study focuses on the land subsidence phenomena manifesting at the Anthemountas basin, at the east of Thessaloniki (Fig. 1).

This area draw the attention of the geo-scientists in 2005 when a series of fractures, causing damages to both buildings and roads, occurred at the Perea village,

on the southern section of the basin's coastal zone. These fractures were attributed to the overexploitation of the aquifers, although they manifested along an active fault (Anthemountas Fault) (Koumantakis et al., 2008). The application of satellite SAR interferometry (InSAR) for the detection of land motion phenomena revealed that beside the Perea village, big parts of the Anthemountas plain and especially the coastal zone subside. Furthermore, a linear pattern of deformations, elongated parallel to the major inactive Thermi Fault, has been observed. The Thermi Fault borders the NE part of the basin and is considered inactive in all former studies (Mountrakis et. al., 1996; Tranos et al., 2003; Karamitrou et al., 2008; Zervopoulou, 2010). The main objectives of the current work are to identify the main causes of the observed ground deformations and to validate the contribution of the remote sensing data on the study of the phenomena.

2 The Anthemountas basin: description of the study area

2.1 Geological background

The broader Thessaloniki area belongs to the NNW–SSE trending alpine Circum Rhodope Belt Thrust System (CRBTS), overthrusting from the east at the Axios geotectonic zone (Peonia subzone). The Circum Rhodope Belt is part of the Inner Hellenic orogen, which is characterized by repeated SW-directed thrust sheets (Tranos et al., 1999, 2003). The pre-alpine and alpine basement, since the Miocene, is subjected to a brittle extensional deformation, forming NW–SE and E–W directed continental-type basins (Pavlides and Kilias, 1987; Tranos, 1998; Tranos et al., 1999, 2003). These basins, among which the Anthemountas basin, are bordered by high-angle normal faults and they have been filled with Neogene and Quaternary sediments.

The geological formations constituting the Anthemountas basin can be distinguished on the Mesozoic bedrock formations, occupying the bordering mountains, the Neogene deposits outcropping at the hilly areas and the foot of the mountains and the Quaternary deposits occupying the plain area (IGME, 1966, 1978a; Rozos et al., 1998;

Anastasiadis et al., 2001). The Mesozoic formations consist of metamorphic (phyllite and gneiss with marble intercalations) and igneous (granite, gabor and peridotite) rocks. The Neogene deposits consist of two sequences, the upper sand and gravel sequence and the lower sandy marls – red clays sequence, outcropping successively along the borders of the basin. The quaternary formations occupy the central part of the plain, with an increasing thickness towards the coastal area.

According to data coming from geotechnical and geophysical studies as well as from the profiles of geotechnical and hydrogeological drills (Thanasoulas, 1983; Rozos et al., 1998; Zervopoulou, 2010), the quaternary formations consist of alternating layers of clastic and fine grained sediments (Fig. 1), generating favourable conditions for the development of an upper phreatic and several successive semi-confined aquifers. Close to the coastline they extend to the depth of 100 to 140 m. Their thickness decreases gradually to the east (Fig. 1).

As already mentioned above, the wider coastal zone is affected by land subsidence phenomena. Focusing at this particular area the quaternary formations can be distinguished in three horizons (Fig. 1). The top horizon, from the surface to a depth of 30 m, consists of coarse to fine sands with gravel intercalations. The second horizon, with a thickness up to 30 m, is occupied by impermeable clay to silty clay layers intercalated by fine sand layers. The third horizon, extending down to the Neogene formations consists of coarse to fine sands with a few clay intercalations. Beneath the quaternary formations extends the Neogene sand and gravel sequence.

The wider Thessaloniki area has recently been affected by the 20 June 1978 destructive earthquake (Papazachos and Papazachou, 1997). Since then, an intense neotectonic and seismological investigation of the broader area has been carried out by numerous researchers (Papazachos et al., 1979, 1982, 2000; Mercier et al., 1983; Mountrakis et al., 1983, 1996; Hatzfeld et al., 1987; Pavlides and Kilias, 1987; Tranos et al., 2003; Karamitrou et al., 2008; Zervopoulou, 2010) providing sufficient information about the distribution of the active faults.

The Anthemounta basin is bordered by two main normal faults, the Anthemounta (F-An) and the Thermi (F-Th) Fault (Fig. 1). The Anthemounta fault with an E–W orientation and a length of 32 km, borders the basin to the south, extending from the Galarino village to the Agelochori peninsula. It is the longest active seismic fault close to the city of Thessaloniki, characterized as active because of the clear morphotectonic indications and the continuous microseismic activity (Zervopoulou, 2010). It constitutes the border line between the rigid Neogene formations and the compressible Quaternary deposits of the plain. Its track is clearly related with the surface ruptures recorded at the Perea village, leading some researchers to the conclusion that they occurred due to the faults activity.

The Thermi fault (F-Th) borders the basin to the north, extending from the Vasilika village to the Mikro Emvolo peninsula. It is a NW–SE oriented fault, dipping to the SW, with a length of approximately 21 km and an extra possible extension of 8 km into the Thermaikos gulf. According to former studies (Tranos et al., 1999; Karamitrou et al., 2008; Zervopoulou, 2010) and because of the lack of activity indications this fault was characterized as inactive.

At the same side of the basin three more active or probably active faults are recorded (Tranos et al., 1999; Karamitrou et. al., 2008; Zervopoulou, 2010). These faults, with a varying length of 5 to 8 km, intersect the Thermi fault presenting an E–W orientation and a south dip direction.

2.2 Hydrogeological setting

Evaluating the profiles from more than 100 water drills (Nagoulis and Loupasakis, 2001) three aquifers systems were distinguished at the plain of the Anthemountas basin. These systems are:

1. The shallow phreatic aquifers system. The shallow aquifers occupy the upper coarse-grained Quaternary deposits and they are mainly replenished by the stream network percolation. Along the coastal zone they extend down to

a maximum depth of 30 m and they are sufficiently separated by the underlying semi-confined aquifers by a thick fine-grained layer (Fig. 1).

2. The semi-confined alternating aquifers. The semi-confined aquifers extend down to depths from 50 to more than 200 m, close to the coastline, occupying the lower Quaternary and the upper sand and gravel sequence of the Neogene deposits. Deeper in the Anthemountas plain (Fig. 1 – Drill Profile 2), where the thickness of the Neogene and Quaternary sediments decreases, this aquifers extend as well down to the fractured Mesozoic formations. They are mainly replenished by the bordering mountains aquifers inflow and also by the shallow aquifer infiltration.

3. The deep confined (artesian) aquifers. Two main aquifers can be distinguished in this category. The first aquifer system extents at the south of the Anthemountas fault, occupies the lower Neogene deposits and the Mesozoic limestone and contains a sub-acidic sparkling mineral water rich in calcium and magnesium (known as Souroti Natural Mineral Water). The other deep confined aquifer is the low enthalpy thermal aquifer gushing out along the Thermi fault close to the homonymous village. These systems do not seem to be affected by the variations of the ground water level of the two shallower aquifer systems.

The rapid urban growth, the industrial development and the intensification of agricultural activity led to the overexploitation of the aquifers. All the villages along the coastline of Anthemountas basin and many other located on the bordering mountains derive drinking water from local low-lying alluvial aquifers. Some of these urbanized areas constitute the most rapidly developing suburbs of Thessaloniki, experiencing both an increasing urbanization trend and a significant population growth in the last few decades. Between 1991 and 2001 an increase of population of about 108 % and 45 % has been recorded in the municipality of Thermaikos and in the whole basin, respectively (WATERinCORE, 2011). Moreover, several industries, economic activities and infrastructures have developed around the Thessaloniki International Airport. Without a proper management, increase of water demand led to an overexploitation of the

groundwater resource. The overexploitation started affecting the ground water conditions since the 90s. As presented at the isopiezometric curves maps referring to the conditions of the deep semi-confined aquifers in 1993 (Fig. 2, left) and 1998 (Fig. 2, right) the ground water level close to the sea was reduced for more than 5 m, during that period. This condition was intensified the following years leading, besides the downgrading of the ground water quality, to the manifestation of land subsidence phenomena. If groundwater overexploitation keeps on going, land subsidence is going to affect rapidly the entire coastal zone of the basin and extend deeper at the Anthemountas plain, wherever the thickness of the quaternary formations is significant, causing great damages both to urban areas and infrastructure.

3 The InSAR technique applied to subsidence analysis

Several methods apply for measuring, mapping and monitoring spatial extent and temporal evolution of regional and local subsidence. Assessment of ground deformation is historically based on conventional geodetic methods (GPS, leveling network above everything else).

Conventional methods for the production of subsidence-affected areas maps rely on materialization of a network of geodetic benchmarks, designed to cover the extension of the likely subsiding area. Repeat surveys of benchmarks, referenced to a stable control point allow the estimation of the deformation extent and rates. These techniques, providing a static picture of the investigated area at each measurements acquisition campaign, are time consuming and resources intensive, since a great deal of time and economic resources are required for timely update. In addition to conventional geodetic monitoring systems, Earth Observation (EO) techniques have successfully demonstrated in the last decades to be highly valuable in measuring land motion in a wide range of application fields (Tralli et al., 2005), including geohazard-related land motions. Their suitability is particularly relevant for wide area studies: when dealing with basin-scale phenomena, the potential of conventional investigation for the analysis of

ground deformation is not comparable to the effectiveness of remote sensing in terms of systematic coverage, timely updating, cost-efficiency and density of measures.

3.1 The PSI approach

EO technologies became even more deeply accepted with the development of Differential Interferometric Synthetic Aperture Radar (DInSAR) techniques. The DInSAR constitutes a remote sensing technique relied on the analysis of phase variations, or interference, between two different radar images (Zebker and Goldstein, 1986; Gabriel et al., 1989; Massonnet and Rabaute, 1993; Massonnet and Feigl, 1998; Rosen et al., 2000), gathered over the same area at different times by the same satellite using the same acquisition mode and properties (beam, orbit, off-nadir angle, etc). The main purpose of DInSAR techniques is to retrieve measurements of the ground displacement that occurred between the two different acquisitions.

The application of satellite conventional DInSAR is limited by temporal and geometrical decorrelation (Zebker and Villasenor, 1992). Also, by using individual interferograms the accuracy on the estimated displacement values can be degraded by atmospheric artifacts (Massonnet and Feigl, 1995).

To overcome the main limitations of single-pair interferogram analysis, many multi-interferometric approaches (under the "family name" Persistent Scatterer Interferometry) have been implemented, processing multi-temporal stacks of satellite SAR images of the same target area. Typically at least 15 images should be available for carrying out a proper PSI analysis. Of course, the larger the number of images the more precise and robust the results.

The main idea underpinning PSI techniques is to discriminate phase contribution related to displacement from those due to atmosphere, topography and noise through the analysis of the so-called PS (Persistent Scatterers) (Ferretti et al., 2000, 2001; Werner et al., 2003). So, Persistent Scatterers are point-like reflecting elements that do not change their spectral response over the entire observation time period. Once the atmospheric effects are estimated and removed, the remaining contribution maps changes

in the satellite-to-target path between the acquisition times of the two images. Over urban fabric, where stable (i.e. phase coherent) reflectors can be identified, LOS (Line of Sight) deformation rate can be estimated with accuracy even better than 0.1 mm yr^{-1} (Colesanti et al., 2003). Unlike DInSAR approach, PSI analyses is designed to generate time-series of ground deformations for individual radar targets (i.e. the Persistent Scatterers, PS), assuming a linear model of deformation (Ferretti et al., 2001; Werner et al., 2003), or exploting algorithm estimating the linear and nonlinear components of the displacement (e.g. Mora et al., 2003).

The accuracy on single measurement in correspondence of each SAR acquisition ranges from 1 to 3 mm (Colesanti et al., 2003). Each measurement is referred temporally and spatially to a unique reference image and to a stable reference point, respectively.

PSInSAR (Ferretti et al., 2000, 2001) was the first algorithm specifically implemented to process long series of SAR images. Following the PSInSAR approach, many multi-interferometric techniques were developed, increasing continuously the interest in PSI techniques. Moreover, the development of the StaMPS (Hooper et al., 2004, 2007) and SqueeSAR techniques (Ferretti et al., 2011) contributed to extend the ability of PSI to natural terrain (Sousa et al., 2010, 2011; Raspini et al., 2011), overcoming the main limitation of the technique.

Nowadays interferometric-based approaches are mature and widely employed by scientific community and practitioners dealing with geo-hazard managements. Since the pioneering studies of Galloway et al. (1998), who introduced InSAR for the detection of aquifer system compaction effects, it was clear that the availability of SAR imagery archives (like the ones provided by European Space Agency, ESA) may support the compilation of subsidence maps, reducing the time for their production and saving economic resources required for timely update. Exhaustive review on the application of remote sensing techniques for mapping subsidence accompanying groundwater overexploitation is given by Galloway and Hoffman (2007) and by Galloway and Burbey (2011).

One of the challenging priority concerning EO data and technology, to guarantee further advances and continuity of the EO-based geohazards services in the next years and to make them more consolidated and accepted by the user communities, includes a broader use of wide-area processing strategies of satellite SAR imagery.

3.2 Used SAR dataset and processing details

Aiming to map the ground deformations on countries and continents based on the PSI technique, in the framework of the ESA Terrafirma project, a Wide Area Product (WAP) has been developed by the German Space Agency (DLR) (Adam et al., 2011).

Nine satellite image frames have been processed to produce a PSI ground motion map covering a 65 000 km^2 wide area of Greece. This WAP product over Greece is based on ERS1/2 images. Among these 9 satellite image frames, track 7_3, made of a dataset of 42 SAR imagery in C-band (5.6 cm wavelength; frequency 5.3 GHz) was employed for the reconstruction of the history and spatial patterns of land subsidence in the Anthemountas basin. These images have been acquired along descending orbits between 10 April 1995 and 1 January 2001 in Stripmap mode, with a temporal resolution of 35 days, which corresponds to the revisiting time of ERS1/2 satellites.

The reference point of the stack – whose selection during the processing activity is of crucial importance – was chosen in the southeast urban fabric of downtown Thessaloniki. Apart from the phase stability throughout the dataset, the reference point is chosen in area assumed unaffected by ground motions. The reference point of the used dataset is located on rigid over consolidated formations of Upper Miocene Age, mainly sandstones, marls and red clays. These rock to hard soil formations can be safely considered as stable, unable to be affected by local scale deformation processes related to hydrogeological factors (fluctuation of the ground water level).

PSI technique uses large stacks of SAR images to generate differential interferograms with respect to one master image. As shown in Fig. 3 the master image for Track 7_3 dataset has been chosen on 31 December 1996, in order to minimize the effects of spatial and temporal baselines.

3.3 Analysis of PSI dataset

The main purpose of the WAP is to implement wide area processing strategies devoted to map countries with the PSI technique. To provide accurately georeferenced, country-scale information on ground motion by using medium resolution SAR sensors (i.e. ERS1/2 with a ground-range and azimuth resolution of 20 m and 5 m, respectively) it is often a challenge.

The validation of the EO measurements accuracy is vitally important. The georeferencing accuracy of the PSI datasets is often difficult to assess, especially when dealing with PSI datasets resulting from ERS processing, due to its low spatial resolution. This fact makes difficult to identify exactly what kind of object is actually acting as "persistent scatterer". The first step for the validation of the PSI datasets was to identify prominent and isolated objects and study the PS point distribution around them. Examples of the georeferencing accuracy are given in Fig. 4. As presented, although the theoretical accuracy for the WAP processing is ±25 m in both X and Y direction, much smaller offset values were actually located. For instance, the PS points along the Thessaloniki breakwater offset to the southwest for approximately 6–8 m, while PSs along Thessaloniki pier fit well with the structure of the pier itself.

The potential of PSI techniques is higher in urban areas, because of the wide availability of bright man-made objects. As expected, in the study area, the density of measurement points is higher for the urban area of Thessaloniki (maximum density up to about 300 PS km^{-2}), as well as over the urban fabric of the Perea village (up to hundred of point km^{-2}). On the contrary over the agricultural and vegetated terrains the density of measurement points is much lower (few point km^{-2}), representing a limiting factor of this technique. Although a relatively limited number of reflectors were retrieved, spatial distribution of ground information is sufficient enough to identify the spatial patterns of deformation.

A frequency histogram has been generated showing the distribution of the 10.061 PS velocity values in the studied region (Fig. 5). The deformation distribution presents two

main components for the time span 1995–2001. First of all, the most common deformation rates are between $-1.5\,\mathrm{mm\,yr^{-1}}$ and $+1.5\,\mathrm{mm\,yr^{-1}}$ (close to the sensitivity of the PSI technique), reflecting motionless areas occupied by Neogene rigid formations and by Mesozoic and Palaeozoic bedrock outcropping on the border of the plain area. The second component (with velocity values, down to $-35\,\mathrm{mm\,yr^{-1}}$), reflects extensive subsiding areas occupied by loose quaternary formations.

LOS deformation rates of each PS point of the dataset have been compared to their elevation a.s.l. (Fig. 5). Motionless targets have been detected at any elevation through the investigated area. Negative values are mainly observed at low elevation (usually less than 100 m a.s.l.). This constraint strongly supports the hypothesis that subsidence largely affects the plain sectors of the Anthemountas River, as a consequence of intense overexploitation of the aquifers located in the alluvial sediments filling the basin.

Examining the spatial distribution of the deformations the PSs points were plotted on a Visual Earth image (Fig. 6). PSs with LOS velocities between $+1.5\,\mathrm{mm\,yr^{-1}}$ and $-1.5\,\mathrm{mm\,yr^{-1}}$ have been considered as stable points. PSs with LOS velocities $< -1.5\,\mathrm{mm\,yr^{-1}}$ and $> +1.5\,\mathrm{mm\,yr^{-1}}$ have been considered as subsiding and uplifting points, respectively. The color scale indicates green points as stable. The gradation from yellow to dark red represents increasing deformation rates. The interpretation of the observed spatial distribution is exhaustively analyzed in the following paragraphs referring to specific parts of the basin.

4 Case studies on specific areas: results and discussions

High PS points density over the urban fabric (Fig. 6) reveals that the city of Thessaloniki and its closest conurbation show very low LOS deformation rates, indicating relatively stable ground conditions during the investigated time period. Indeed, large parts of the urban fabric are built over Neogene rigid formations, mainly compact sandstones, marls and over consolidated red silty clays, which outcrop extensively in the urban areas.

Nevertheless, at the nearby Anthemountas basin the conditions regarding the deformations are different. Unstable areas clearly manifest in the central-lower part of the basin, presenting a mean deformation rate of $10\,\mathrm{mm\,yr^{-1}}$. The measured subsidence rates increase towards the coastline (moving from south-east to north-west), where the thickest sequences of compressible Quaternary layers occur. Considering the decreasing drawdown of the semi-confined aquifers piezometric level as well as the decreasing thickness of the loose Quaternary formations towards Vasilika (Fig. 2), the deformations are expected to nullify accordingly. The lack of PSI data concerning the plain area between the subsidence bowl, close to the coastline, and Vasilika village does not allow any further estimation about the extension of the attenuating subsidence phenomenon to the south-east.

Issues of particular interest are presented by the airport area, with several points exceeding $20\,\mathrm{mm\,yr^{-1}}$, and by the Perea village in the Thermaikos municipality, with LOS deformation rates up to $10–15\,\mathrm{mm\,yr^{-1}}$. These subsidence phenomena were first noticed in 2005–2006, where a series of fractures, causing damages to both buildings and infrastructures, occurred at the Perea village. Since then, no further indications have been recorded at the rest of the area, and the above described extension of the deformations distribution was never recorded or studied by means of any other technique. From the first moment the phenomena occurred at the Perea village were attributed to the overexploitation of the aquifers (Koumantakis et al., 2008) and as mentioned in Sect. 2.2 the dominant process triggering the observed ground deformations along the central part of the basin's coastal zone seems to be the same.

Besides the subsidence bowl close to the coastline, a second pattern of deformation has been detected parallel to the Thermi normal fault bordering the northeast part of the basin. These deformations are of particular interest as the current fault is considered by several researchers as inactive.

4.1 Thessaloniki airport area

Located at the south of Anthemountas River outfall (Fig. 1), about 15 km SE of the city centre of Thessaloniki, the International Airport "Macedonia" is the largest state owned airport in Greece. With 3.9 million passengers during 2010 it is the main airport of northern Greece and serves the city of Thessaloniki, the surrounding cities of the region and many popular tourist destinations. Considering the geological setting, the sensitive anthropogenic context and the logistic importance of this infrastructure, the analysis of surface deformation is a priority. As highlighted by Ge et al. (2009), potential damages of such infrastructures are not only loss of money but also loss of significant landmark in the world.

In order to deeply understand the deformation pattern along infrastructures such as airports, characterized by large linear extent, a monitoring technique coupling wide coverage and high precision is required. During the last years, interest and attention on these problems increased, and analysis of linear infrastructures stability has been successfully carried out with PSI technique (Pigorini et al., 2010).

Subsidence of about 5–15 mm yr^{-1} has been observed in the airport area, with several points exceeding 20 mm yr^{-1} along the two runway areas. Observed subsidence is without any doubt related to the terrain compaction accompanying the excessive groundwater withdrawal occurred in the Anthemountas plain. Indeed, the airport area is located within a wider scale subsidence bowl which affects a large extension of the basin (Fig. 6).

In order to better investigate the subsidence zone along runways areas, two buffer zones of 500 m have been considered. Two sets of point-wise PSs have been extracted within the buffer zones (Fig. 7) to create interpolated subsidence rate maps for both runways areas (about 2400 m in length).

The two sets of scattered points are first used to extend the information (i.e. to interpolate) to less-density areas, calculating values to unmeasured location through the IDW (Inverse Distance Weighted) method (Shepard, 1968). To result a spatially

continuous surface, IDW method uses a weighted average of the available known points, taking into higher account given values at nearby locations. The weights decrease as the distance between the known point and the interpolation point increases.

Due to the mono-dimensional characteristic of the radar measurements, PSI technique can estimate only the sensor-to-target displacement, i.e. the projection along the LOS (VLOS) of the real motion. Assuming the occurrence of predominant vertical motion in the Anthemountas plain (as suggested by Raspini et al., 2012 for groundwater exploitation-related ground subsidence), the vertical deformations (Vv) can be estimated solving the following formula: $Vv = VLOS/\cos\theta$. Considering the ERS1/2 satellites, the look angle θ is about 23°. The relation above corresponds to an increment of the VLOS of about 8.6 %.

By interpolating the mean velocity values retrieved by PSI technique within the buffer zone, two subsidence profiles can be generated (Fig. 8), showing the distribution and magnitude of subsidence along the runway areas of the Thessaloniki airport. Profiles correspond to the longitudinal lines along the center of the runways. The major subsidence zone could be found in the central part of both profiles (distance range between 1100 and 1800 m), close to the section where the two runways cross each other. The maximum subsidence rate values at this particular section reach the 23 mm yr^{-1}.

Linear infrastructures, like airports, are mainly affected by the manifestation of differential displacements, and less affected by the absolute values of subsidence. Differential displacements are mainly caused by lateral variations on the thickness of the compressible soil layers constituting the site (imposed by the stratigraphy or the tectonic of the area) as well as by uneven fluctuations of the ground water piezometric surface. Examining the differential deformations calculated along the runways, Fig. 8 clearly indicates a non-uniform subsidence. The higher differential setting has been recorded along the WNW–ESE oriented runway with a value of 40 mm/100 m. In agreement with the maximum subsidence rate section, the highest differential displacements occur close to the intersection of the two runways. At this particular case study the differential displacements are caused by lateral variations on the thickness of the compressible

soil layers of the deltaic Quaternary foundation formations. Uneven fluctuations of the ground water piezometric surface cannot be expected as only two low consumption wells operate at the entire airport landholding.

4.2 Perea village

PSI results of Fig. 6 reveal that the coastal area of the Perea village (Thermaikos municipality) shows very low LOS deformation rates, ranging between −1.5 and 1.5 mm yr^{-1}, indicating relatively stable ground conditions since 1995. Nevertheless, in the southern part of the urban area (upper Perea) subsidence can be observed, with maximum LOS deformation rates up to 10–15 mm yr^{-1} (Fig. 9).

The potential of repeat-pass space-borne SAR interferometry can be exploited not only to map the extension of affected areas but also to evaluate their deformation history. Displacement time series available for each PS in the area of interest are ideally suited for monitoring temporally continuous geohazard-related ground motions. Example of time series, referring to three Permanent Scatterers located in the Perea's section affected by ground motion, are reported in Fig. 10.

The extraction of groundwater is considered as the main factor causing the land deformation measured, from April 1995 to January 2001, in the village of Perea. The most pernicious consequence of water level drawdown and relative terrain compaction has been the development, in 2005–2006, of a series of fractures affecting the urban fabric. Surface ruptures deformed streets pavement and caused serious damages on buildings, making some of them uninhabitable and forcing their demolishment (Fig. 11).

The abovementioned ground ruptures extend parallel to the coastline, approximately along an E–W direction, dipping towards north. They extend for a length of about one kilometre along the scarp of the Anthemountas fault, defining the boundary between the thick Quaternary alluvial deposits and the Neogene formation, delimiting the subsiding basin. Actually the manifestation of the ruptures at this particular location, along the scarp of the fault, has been arranged by the abovementioned boundary.

The groundwater withdrawal affecting the area takes place for the last twenty years. Analysis of the hydrogeological conditions of the village of Perea is included in Koumantakis et al. (2008), who first identified the overexploitation of confined aquifer as the main cause of the observed ground deformation. As mentioned above, the Quaternary alluvial deposits in the Perea wide area are characterized by both phreatic and semi-confined aquifers (Nagoulis and Loupasakis, 2001). The continuous increase on water demand of the Thermaikos municipally is exclusively covered by the ground water exploitation. A great number of public and private wells are in operation in the wider area. The public wells are deep, reaching down to depths from 120 to 380 m, providing large quantities of good quality drinking water. Despite the public network for water supply and distribution, several private and usually uncontrolled water wells have been drilled without careful management.

Besides the ground water drawdown taking place along the coastal zone of the Anthemountas basin, the narrow area affected by the surface ruptures is located inside the intersecting depression cones of three public and probably several unknown private wells. The locations of the three public wells (G1, G2 and G3) are clearly indicated in Fig. 9 and as presented they are located only a few tens of meters away from the ruptures. So, it is clear that the narrow area affected by the ruptures is subjected to an extra ground water drawdown, amplifying the subsidence mechanism, active in large parts of the Anthemountas basin.

The intensiveness of the ground water drawdown can be seen in the graphs of Fig. 12 presenting the drawdown progress in two of the aforementioned wells, G1 and G3. According to the graph, at the G1 well the drawdown from November of 1996 to October of 2006 was 22 m (mean annual rate of 2.2 m), whereas in the G3 well, the drawdown from September of 1998 to September of 2006 reached the value of 11.5 m (mean annual rate of 1.44 m).

Tensile ruptures in Perea village are the ultimate effects of water terrain compaction related to water level decline. Other visible traces of subsidence, like well-casing protrusion have been reported northern to surface ruptures. Besides that, no other effects

related to the groundwater withdrawal can be clearly detected without analyzing PSI data.

4.3 Thermi fault

Besides the aforementioned deformations related with the overexploitation of the aquifers at the lower section of the basin, high deformation rates are also observed, with a linear pattern, along the northeast border of the Anthemountas basin. This second pattern of deformation has been detected to coincide with the NW–SE oriented trace of the Thermi fault, a normal fault bordering the basin (Fig. 13). As mentioned at the geological background paragraph this fault, based on former studies (Tranos et al., 1999; Karamitrou et al., 2008; Zervopoulou, 2010) as well as on the lack of earthquakes recordings, was characterized as inactive.

According to the PSI data along the fault line an excessive mean deformation rate of 5–7 mm yr^{-1}, with peak values up to 10 mm yr^{-1}, is observed (Fig. 14). The detailed distribution of the LOS deformation rates indicates that the peak deformation values are mainly observed at the intersections of the main fault with the three E–W oriented active faults. The wide section, at the beginning of the curve, presenting deformations up to 20 mm yr^{-1} correspond to the land subsidence area along the coastal zone.

Hence, the evaluation of the PSI data revealed a possible activity at the Thermi fault. This activity seems to be amplified at the intersections of the fault itself with the E–W oriented active faults and it also seems to be concealed by the land subsidence deformations. Furthermore the possibility of a tectonic component at this particular linear deformation pattern is supported by the fact that the subsiding PS points cover the entire mapped length of the fault, even in areas where no land subsidence due to the overexploitation of the aquifers is expected (SE of Vasilika). A more accurate estimation of the displacement gradient across the fault cannot be done by the available PSI data because the PS points were unevenly distributed at the two sides of the fault and no clear pattern of deformation can be identified. Similar studies evaluating

successfully the activity of faults use much denser and well distributed PSI datasets (Cigna et al., 2011; Parcharidis et al., 2009, 2013).

Density and distribution of PS targets offer a synoptic view of the linear deformation patter along the NE side of the Anthemountas basin, indicating that a possible tectonic component might be included at this deformation. Actually, considering the fact that the basin is still subjected to a brittle extensional deformation, a low seismicity creep-like deformation can be justified at the current fault.

5 Discussion

Analysis of deformation affecting the Anthemountas basin proved the importance of early detection and measuring of ground movements related to subtle phenomena like subsidence. Indeed, the mitigation of land subsidence and related effects is very difficult at a late stage. Models explaining and simulating the expected ground subsidence induced by aquifers exploitation are summarized by Galloway and Burbey (2011) and applied by Loupasakis and Rozos (2009) and Herrera et al. (2009).

The compaction of the formations is irreversible and furthermore the progress of the deformations cannot be stopped rapidly by just stopping the overexploitation of the aquifers. The artificial recharge of the aquifers does not seem to give a solution to the problem as the consolidated formations present reduced transmissivity values delaying the restoration of the ground water pore pressure and as a result the deceleration of the deformations. Certainly, the best way to prevent the consequences of the land subsidence is to block their progress before they start causing damages. The integrated water resource management is the best way to deal with early stage subsidence. The only problem, as already mentioned above, is that the deformations can take place for several years before being noticed. In that case, this study proved that SAR interferometry and in particular PSI techniques are valuable tools for the early stage detection of the vertical deformations caused by the overexploitation of the aquifers.

Furthermore, main outcomes from the deformation analysis at the Thessaloniki airport give the opportunity to make some considerations about the effectiveness of PSI techniques for mapping and monitoring deformation pattern of linear transportation networks (i.e. railways, highways, main roads), aerial utilities infrastructures (aqueducts, oleoduct and pipe networks for transportation of goods in general) and underground excavations (metro and tunnel constructions).

First of all it is worth noticing the density of the two sets of measurement points created for the analysis: (a) the buffer dataset created for the NNW–SSE oriented runway area includes 122 PSs, with a density of 81 PS km^{-2} and (b) the buffer dataset for the WNW–ESE includes 149 PSs, with a density of 96 PS km^{-2}. Conventional geodetic networks, despite their robustness and reliability, are not able to provide such a large density of measurement points, as PSI technique does. So, the numerous measurement points, coupled with the mm yr^{-1} accuracy, enhance the overall understanding and confidence on ground motion occurring in the investigated area, improving the spatial and temporal characterization of the subsidence.

Full coverage of the runway areas cannot be expected with medium resolution satellites like ERS1/2 used in this analysis. Azimuth and range resolutions (along and perpendicular to the flight direction, respectively) of the SAR sensor installed on the ERS1/2 platform are quite poor. The resolution mainly depends on the bandwidth and on the length of radar antenna. The ERS SAR sensor has a bandwidth of 15.6 MHz (wavelength of 5.6 cm), and an antenna length of 10 m. Consequently, the ground range resolution is about 20 m and the azimuth resolution is 5 m. Taking into account the flight path almost parallel to Earth's meridians, east–west oriented linear structures are imaged poor due to the lower range resolution. On the contrary linear structures with a north–south oriented component are expected to be more coherent in the SAR images, due to the higher azimuth resolution.

Due to the high revisiting time (24–35 days) PSI data cannot be used as a real-time monitoring tool neither during construction works, nor for timely updated stability analysis of existing structures. This consideration stands for both previously in

orbit satellites (the European ERS1/2 and Envisat) and still operating satellites (the Canadian Radarsat1/2). Nevertheless, since 2008, high resolution imagery acquired by two X-band (3.1 cm of wavelength) radar satellite sensors are available: (a) the Italian COSMO-SkyMed SAR constellation of satellites, and (b) the German TerraSAR-X satellite.

With an increased bandwidth of 300 MHz more coherent targets can be retrieved, providing a higher density of PS points. A better ground resolution (up to 1 m in both azimuth and range direction) and a reduced revisiting time (from 4 to 11 days), are ideally designed for local scale analysis of deformation patterns and for investigating their temporal evolution. Furthermore, given their intrinsic characteristics, this generation of radar sensors allows monitoring faster movements. Taking into account the wavelength and the revisiting time, the higher discernible velocity is up to 25.5 cm yr^{-1}, with respect to 14.6 cm yr^{-1} with the ERS1/2 system. The enhanced characteristics of the new generation of SAR sensors have improved the capability of PSI technique for land motion mapping (Crosetto et al., 2010).

Better spatial resolution, wider applicability to more recent, complex ground movements gave the unique opportunity for a more effective use of SAR data also as monitoring tool in emergency situations (Covello et al., 2010).

Moreover, in the next few years, the launch of new satellite systems (Sentinel 1 and Radarsat Constellation Mission) will further facilitate the research and analysis of land surface phenomena, ensuring the continuity of C-band SAR data (Snoeij et al., 2008) and coupling wide coverage, high precision and short revisiting time.

This study presented new possible applications of the WAP mapping on the field of active fault monitoring. InSAR techniques can substantially contribute on overcoming the difficulties of detecting and monitoring active faults, especially in urbanized environments where the density of the PSI data can be really high. The correlation of ground deformation, measured by InSAR, with active tectonics can considerably assist in assessing seismic hazard and risk. As InSAR has the unique advantage of improving its

performance with areas becoming more urbanized, it holds even greater potential for the future (Mouratidis et al., 2011).

6 Conclusion

The potential of SAR interferometry has been exploited through the innovative WAP approach, recently implemented by DLR and aimed at measuring land deformation over large areas.

Interferometric results acquired in 1995–2001 by ERS1/2 satellites has been analyzed at a basin scale in order to investigate spatial patterns of land motion in the wider Anthemountas plain. The WAP results turned out to be a valuable tool for the characterization of the land subsidence in the wider plain as, up to now, the only indications of land subsidence phenomena were identified at the village of Perea, affected in 2005–2006 by a series of tensile ground ruptures due to excessive groundwater withdrawal. The PSI data revealed that not only Perea but also large parts of the lower areas of the Anthemountas plain, where the International airport of Thessaloniki is located, are affected by land subsidence phenomena.

Besides the land subsidence-related deformations, the WAP revealed movements probably related with active tectonics. The linear pattern of PS along the "inactive" Thermi fault provides new data for the possible re-evaluation of the tectonic model of the basin.

The detection of subsidence phenomena at an initial stage is extremely important, as further extension of the affected area and damages on settlements and infrastructure can be prevented.

Acknowledgements. The Terrafirma Extension project has funded the SAR imagery processing as well as the geological interpretation presented in this paper. The project is one of the many services supported by the Global Monitoring for Environment and Security (GMES) Service Element Programme, promoted and financed by ESA. The authors gratefully acknowledge the German Aerospace Centre (DLR) for having processed the SAR data.

References

Adam, N., Rodriguez Gonzalez, F., Parizzi, A., and Liebhart, W.: Wide area persistent scatterer Interferometry, Proceedings of IGARSS, Vancouver, Canada, 2011.

Anastasiadis, A., Raptakis, D., and Pitilakis, K.: Thessaloniki's detailed microzoning: subsurface structure as basis for site response analysis, Pure Appl. Geophys., 158, 2597–2633, 2001.

Andronopoulos, V., Rozos, D., and Hatzinakos I.: Subsidence phenomena in the industrial area of Thessaloniki, Greece, in: Land Subsidence, vol. 200, edited by: Johnson, A., IAHS Publishers, Wallingford, Oxfordshire, 59–69, 1991.

Cigna, F., Osmanoglu, B., Cabral-Cano, E., Dixon, T. H., Avila-Olivera, J. A., Garduno-Monroy, V. H., DeMets, C., and Wdowinski, S.: Monitoring land subsidence and its induced geological hazard with Synthetic Aperture Radar Interferometry: a case study in Morelia, Mexico, Remote Sens. Environ., 117, 146–161, doi:doi:10.1016/j.rse.2011.09.005, 15 February 2012.

Colesanti, C., Ferretti, A., Prati, C., and Rocca, F.: Monitoring landslides and tectonic motion with the Permanent Scatterers technique, Eng. Geol., 68, 3–14, 2003.

Covello, F., Battazza, F., Coletta, A., Lopinto, E., Fiorentino, C., Pietranera, L., Valentini, G., and Zoffoli, S.: COSMO-SkyMed an existing opportunity for observing the Earth, J. Geodynam., 49, 71–180, 2010.

Crosetto, M., Monserrat, O., Iglesias, R., and Crippa, B.: Persistent Scatterer interferometry: potential, limits and initial C- and X-band comparison, Photogram. Eng. Remote Sens., 76, 1061–1069, 2010.

Dimitrakopoulos, D. and Koumantakis, I.: Big troughs creation on the surface from covered karst activation due to drawdown caused by overpumping for mine protection and in dry periods, Proceedings of 3rd Hydrogeological Congress, Herakleion, 393–407, 3–5 November 1995.

Ferretti, A., Prati, C., and Rocca F.: Nonlinear subsidence rate estimation using Permanent Scatterers in differential SAR interferometry, IEEE T. Geosci. Remote, 38, 2202–2212, 2000.

Ferretti, A., Prati, C., and Rocca F.: Permanent Scatterers in SAR interferometry, IEEE T. Geosci. Remote, 39, 8–20, 2001.

Ferretti, A., Fumagalli, A., Novali, F., Prati, C., Rocca, F., and Rucci, A.: A new algorithm for processing interferometric data-stacks: SqueeSAR™, IEEE T. Geosci. Remote, 99, 1–11, 2011.

Gabriel, A. K., Goldstein, R. M., and Zebker, H. A.: Mapping small elevation changes over large areas: differential radar interferometry, J. Geophys. Res., 94, 9183–9191, 1989.

Galloway, D. L. and Burbey, T. J.: Review: regional land subsidence accompanying groundwater extraction, Hydrogeol. J., 19, 1459–1486, 2011.
Galloway, D. L. and Hoffmann, J.: The application of satellite differential SAR interferometry-derived ground displacements in hydrogeology, Hydrogeol. J., 15, 133–154, 2007.
Galloway, D. L., Hudnut, K. W., Ingebritsen, S. E., Phillips, S. P., Peltzer, G., Rogez, F., and Rosen, P. A.: Detection of aquifer system compaction and land subsidence using interferometric synthetic aperture radar, Antelope Valley, Mojave Desert, California, Water Resour. Res., 34, 2573–2585, 1998.
Ge, D., Wang, Y., Zhang, L., Xia, Y., Wang, Y., and Guo, X.: Using permanent scatterer InSAR to monitor land subsidence along High Speed Railway – the first experiment in China, Proceedings of Fringe, Frascati, Italy, 30 November – 4 December 2009.
Hatzfeld, D., Christodoulou, A. A., Scordilis, E. M., Panagiotopoulos, D., and Hatzidimitriou, P. M.: A microearthquake study of the Mygdonian graben (northern Greece), Earth Planet. Sci. Lett., 81, 379–396, 1987.
Herrera, G., Fernández, J. A., Tomás, R., Cooksley, G., and Mulas, J.: Advanced interpretation of subsidence in Murcia (SE Spain) using A-DInSAR data – modelling and validation, Nat. Hazards Earth Syst. Sci., 9, 647–661, doi:10.5194/nhess-9-647-2009, 2009.
Hooper, A., Zebker, H. A., Segall, P., and Kampes, B.: A new method for measuring deformation on volcanoes and other natural terrains using InSAR persistent scatterers, Geophys. Res. Lett., 31, L23611, doi:10.1029/2004GL021737, 2004.
Hooper, A., Segall, P., and Zebker, H. A.: Persistent scatterer interferometric synthetic aperture radar for crustal deformation analysis, with application to Volcán Alcedo, Galápagos, J. Geophys. Res., 112, B07407, doi:10.1029/2006JB004763 2007.
I.G.M.E. – Institute of Geological and Mineralogical Exploration: Geological Map of Greece, Scale 1 : 50 000, Epanomi Sheet, IGME, Athens, 1966.
I.G.M.E. – Institute of Geological and Mineralogical Exploration: Geological Map of Greece, Scale 1 : 50 000, Thessaloniki, Thermi and Vasilika Sheets, IGME, Athens, 1978a.
I.G.M.E. – Institute of Geological and Mineralogical Exploration: Geological Map of Greece, Scale 1 : 500 000, IGME, Athens, 1978b.
Ikehara, M. E.: Global positioning system surveying to monitor land subsidence in Sacramento Valley, CA, USA, Hydrol. Sci. J., 39, 417–429, 1994.
Kaplanides, A. and Fountoulis, D.: Subsidence phenomena and ground fissures in Larissa, Karla basin, Greece: their results in urban and rural environment, in: Eng. Geol. Environ.,

edited by: Marinos, P., Koukis, G., Tsiambaos, G., and Sambatakakis, G., Balkema, Rotterdam, 729–735, 1997.
Karamitrou, A., Roumelioti, Z., and Kiratzi, A.: Stochastic ground motion simulations from active tectonic structures in the vicinity of the city of Thessaloniki, in: Proceedings of the 3rd Pan-Hellenic conference Earthquake Engineering and Engineering Seismology, Pub. No. 2082, Athens, Greece, 5–7 November 2008.
Kontogianni, V., Pytharouli, S., and Stiros, S.: Ground subsidence, Quaternary faults and vulnerability of utilities and transportation networks in Thessaly, Greece, Environ. Geol., 52, 1085–1095, 2007.
Koumantakis, I., Rozos, D., and Markantonis, K.: Ground subsidence in Thermaikos municipality of Thessaloniki County, Greece, International Conference Gro-Pro – Ground Water Protection – Plans and Implementation in a North European Perspective, 1, Korsør, Denmark, 177–184, 15 to 17 September 2008.
Loupasakis, C. and Rozos, D.: Land subsidence induced by water pumping in Kalochori village (north Greece) – simulation of the phenomenon by means of the finite element method, Q. J. Eng. Geol. Hydroge., 42, 369–382, 2009.
Massonnet, D. and Feigl, K. L.: Discrimination of geophysical phenomena in satellite radar interferograms, Geophys. Res. Lett., 22, 1537–1540, doi:10.1029/95GL00711, 1995.
Massonnet, D. and Feigl, K. L.: Radar interferometry and its application to changes in the Earth's surface, Rev. Geophys., 36, 441–500, doi:10.1029/97RG03139 1998.
Massonnet, D. and Rabaute T.: Radar interferometry: limits and potential, IEEE T. Geosci. Remote, 31, 455–464, 1993.
Mercier, J. L., Carey-Gailhardis, E., Mouyaris, N., Simeakis, K., Roundoyannis, T., and Anghelidhis, C.: Structural analysis of recent and active faults and regional state of stress in the epicentral area of the 1978 Thessaloniki earthquakes (northern Greece), Tectonics, 2, 577–600, 1983.
Mertikas, S. P. and Papadaki, E. S.: Radar Intererferometry for Monitoring Land Subsidence due to over-pumping Ground Water in Crete, Greece, Proceedings of the Fringe Workshop, Frascati, Italy, from 30 November to 4 December 2009.
Mora, O., Mallorquí, J. J., and Broquetas, A.: Linear and nonlinear terrain deformation maps from a reduced set of interferometric SAR images, IEEE T. Geosci. Remote, 41, 2243–2253, 2003.

Mountrakis, D., Psilovikos, A., and Papazachos, B. C.: The geotectonic regime of the Thessaloniki earthquakes, in: The Thessaloniki, Northern Greece, Earthquake of 20 June 1978 and Its Seismic Sequence, edited by: Papazachos, B. C. and Carydis, P. G., Technical Chamber of Greece, 11–27, Thessaloniki, Greece, 1983.

Mountrakis, D., Kilias, A., Pavlides, S., Sotiriadis, L., Psilovikos, A., Astaras, T., Vavliakis, E., Koufos, G., Dimopoulos, G., Soulios, G., Christaras, V., Skordilis, M., Tranos, M., Spyropoulos, M., Patras, D., Syrides, G., Lamprinos, N., and Laggali, T.: Neotectonic Map of Greece, Scale 1 : 100 000, Sheets: Thessaloniki, E.P.P.O. – Earthquake Planning and Protection Organization, Athens, 1996.

Mouratidis, A., Costantini, F., and Votsis, A.: Correlation of DInSAR deformation results and active tectonics in the city of Thessaloniki (Greece), JURSE Conference, Munich, Germany, 421–424, doi:10.1109/JURSE.2011.5764809, 2011.

Nagoulis, A. and Loupasakis, C.: Hydrogeological conditions of the plain area of the Anthemounta basin (Macedonia, Greece), Bull. Geol. Soc. Gre., 34, 1859–1868, 2001.

Papazachos, B. C. and Papazachou, C.: The Earthquakes of Greece, Ziti Publications, Thessaloniki, 1997.

Papazachos, B. C., Mountrakis, D., Psilovikos, A., and Leventakis, G.: Surface fault traces and fault plane solutions of May–June 1978 major shocks in the Thessaloniki area, Tectonophysics, 53, 171–183, 1979.

Papazachos, B. C., Tsapanos, T. M., and Panagiotopoulos, D. G.: A premonitory pattern of earthquakes in northern Greece, Nature, 296, 232–235, 1982.

Papazachos, C. B., Soupios, P., Savvaidis, A., and Roumelioti, Z.: Identification of small-scale active faults near metropolitan areas: an example from the Asvestochori fault near Thessaloniki, Proceedings of the XXXII ESC General Assembly, Lisbon, Portugal, 221–225, 10–15 September 2000.

Parcharidis, I., Foumelis, M., Kourkouli, P., and Wegmuller, U.: Persistent Scatterers InSAR to detect ground deformation over Rio-Antirio area (western Greece) for the period 1992–2000, J. Appl. Geophys., 68, 348–355, 2009.

Parcharidis, I., Kourkouli, P., Karymbalis, E., Foumelis M., and Karathanassi V.: Time series synthetic aperture radar interferometry for ground deformation monitoring over a small scale tectonically active deltaic environment (Mornos, central Greece), J. Coast. Res., 29, 2, 325–338, doi:10.2112/JCOASTRES-D-11-00106.1, 2013

Pavlides, S. B. and Kilias, A. A.: Neotectonic and active faults along the Serbomacedonian zone (Chalkidiki, N. Greece), Ann. Tecton., 1, 97–104, 1987.

Phien-wej, N., Giao, P. H., and Nutalaya, P.: Land subsidence in Bangkok, Thailand, Eng. Geol., 82, 187–201, 2006.

Pigorini, A., Ricci, M., Sciotti, A., Giannico, C., and Tamburini, A.: Satellite remote-sensing PSInSAR^{TM} technique applied to design and construction of railway infrastructures, Ingegneria ferroviaria, Anno LXV(10), 9, 729–757, 2010.

Psimoulis, P., Ghilardi, M., Fouache, E., and Stiros, S.: Subsidence and evolution of the Thessaloniki plain, Greece, based on historical levelling and GPS data, Eng. Geol., 90, 55–70, 2007.

Raspini, F., Moretti, S., and Casagli, N.: Landslide mapping using SqueeSAR data: Giampilieri (Italy) case study, Proceedings of the Second World Landslide Forum, Rome, Abstr. no. 664, 3–9 October 2011.

Raspini, F., Cigna, F., and Moretti, S.: Multi-temporal mapping of land subsidence at basin scale exploiting Persistent Scatterer Interferometry: case study of Gioia Tauro plain (Italy), J. Maps, 8, 514–524, 2012.

Raucoules, D., Parcharidis, I., Feurer, D., Novalli, F., Ferretti, A., Carnec, C., Lagios, E., Sakkas, V., Le Mouelic, S., Cooksley, G., and Hosford, S.: Ground deformation detection of the greater area of Thessaloniki (Northern Greece) using radar interferometry techniques, Nat. Hazards Earth Syst. Sci., 8, 779–788, doi:10.5194/nhess-8-779-2008, 2008.

Rosen, P. A., Hensley, S., Joughin, I. R., Li, F. K., Madsen, S. N., Rodriguez, E., and Goldstein, R. M.: Synthetic aperture radar interferometry, IEEE T. Geosci. Remote, 88, 333–382, doi:10.1109/5.838084, 2000.

Rozos, D., Hatzinakos, I., and Apostolidis, E.: Engineering Geological Map of Thessaloniki wider area, Scale 1 : 25 000, I.G.M.E., Athens, 1998.

Rozos, D., Sideri, D., Loupasakis, C., and Apostolidis, E.: Land subsidence due to excessive groundwater withdrawal, a case study from Stavros-Farsala site, west Thessaly Greece, Proceedings of the 12th International Congress, Patras, Bull. Geol. Soc. Gre., 4, 1850–1857, 19–22 May 2010.

Shepard, D.: A two-dimensional interpolation function for irregularly-spaced data, Proceedings of the 1968 ACM National Conference, 517–524, New York 27–29 August 1968.

Snoeij, P., Attema, E., Davidson, M., Floury, N., Levrini, G., Rosich, B., and Rommen, B.: Sentinel-1, the GMES radar mission. Proc. IEEE Radar Conference, 1–5, Rome, Italy, 26–30 May 2008.

Soulios, G., Tsapanos, T., Voudouris, K., Kaklis, T., Mattas, C., and Sotiriadis, M.: Ruptures on surface and buildings due to land subsidence in Anargyri village (Florina Prefecture, Macedonia), Environ. Earth Sci., 5, 505–512, 2011.

Sousa, J. J., Ruiz, A. M., Hanssen, R. F., Bastos, L., Gil, A. J., Galindo-Zaldívar, J., and Sanz de Galdeano, C.: PS-InSAR processing methodologies in the detection of field surface deformation – study of the Granada basin (Central Betic Cordilleras, southern Spain), J. Geodynam., 49, 181–189, 2010.

Sousa, J. J., Hooper, A. J., Hanssen, R. F., Bastos, L. C., and Ruiz, A. M.: Persistent Scatterer InSAR: a comparison of methodologies based on a model of temporal deformation vs. spatial correlation selection criteria, Remote Sens. Environ., 115, 2652–2663, 2011.

Stiros, S. C.: Subsidence of the Thessaloniki (northern Greece) coastal plain, 1960–1999, Eng. Geol., 61, 243–256, 2001.

Thanasoulas, K.: Geophysical study of Anthemountas area, Unpublished technical report, I.G.M.E., Athens, 1983 (in Greek).

Tralli, D. M., Blom, R. G., Zlotnicki, V., Donnellan, A., and Evans, D. L.: Satellite remote sensing of earthquake, volcano, flood, landslide and coastal inundation hazards, J. Photogram. Remote Sens., 59, 185–198, 2005.

Tranos, M. D.: Contribution to the study of the neotectonic deformation in the region of Central Macedonia and North Aegean, Ph.D. thesis, University of Thessaloniki, Thessaloniki, 1998, (in Greek).

Tranos, M. D., Kilias, A. A., and Mountrakis, D. M.: Geometry and kinematics of the Tertiary post-metamorphic Circum Rhodope Belt Thrust System (CRBTS), northern Greece, Bull. Geol. Soc. Gre., 33, 5–16, 1999.

Tranos, M. D., Papadimitriou, E. E., and Kilias, A. A.: Thessaloniki–Gerakarou Fault Zone (TGFZ): the western extension of the 1978 Thessaloniki earthquake fault (northern Greece) and seismic hazard assessment, J. Struct. Geol., 25, 2109–2123, 2003.

WATERinCORE: Sustainable Water Management through Common Responsibility enhancement in Mediterranean River Basins – Strategic Water Management Plan for Anthemountas River Basin, Agence de Developpment de Thessaloniki Oriental, ANATOLIKI S. A., Kentriki Makedonia (Greece), 2011.

Werner, C., Wegmuller, U., Strozzi, T., and Wiesmann, A.: Interferometric point target analysis for deformation mapping, Proceedings of IGARSS, 4362–4364, Toulouse, France, 21–25 July 2003.

Zebker, H. A. and Goldstein, R. M.: Topographic mapping from interferometric synthetic aperture radar observations, J. Geophys. Res., 91, 4993–4999, 1986.

Zebker, H. A. and Villasenor, J.: Decorrelation in interferometric radar echoes, IEEE T. Geosci. Remote, 30, 950–959 doi:10.1109/36.175330, 1992.

Zervopoulou, A.: Neotectonic Faults of the Wide Area of Thessaloniki in association with foundation Soils, Ph.D. thesis, University of Thessaloniki, Thessaloniki, 2010 (in Greek).

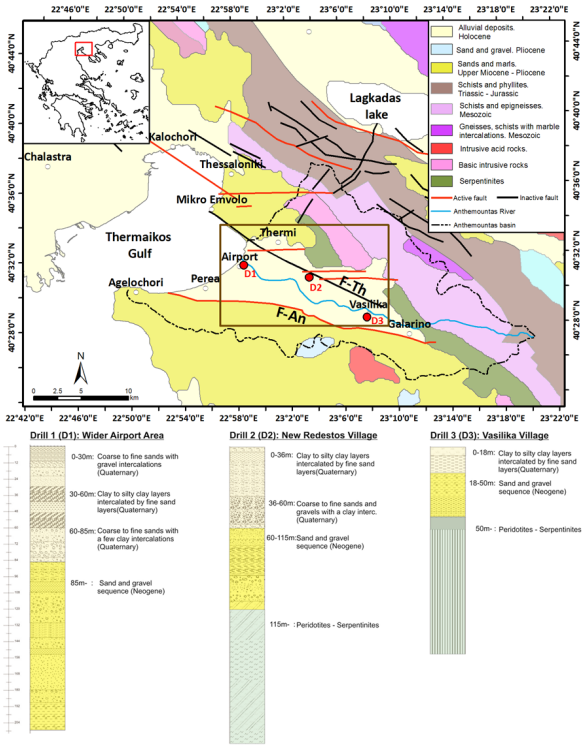

Fig. 1. Location and geological map of the Anthemountas basin. Geology modified from I.G.M.E. (1978b). Three characteristic drill profiles present the vertical distribution of the geological formations from the coastline to Vasilika village. The rectangular indicates the area presented in Fig. 2.

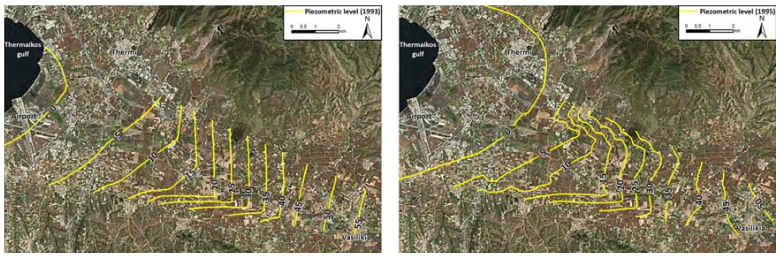

Fig. 2. Isopiezometric curves of the deep semi-confined aquifers system of the area within the brown inset of Fig. 1. May 1993 (left) and May 1998 (right). Data from Nagoulis and Loupasakis (2001).

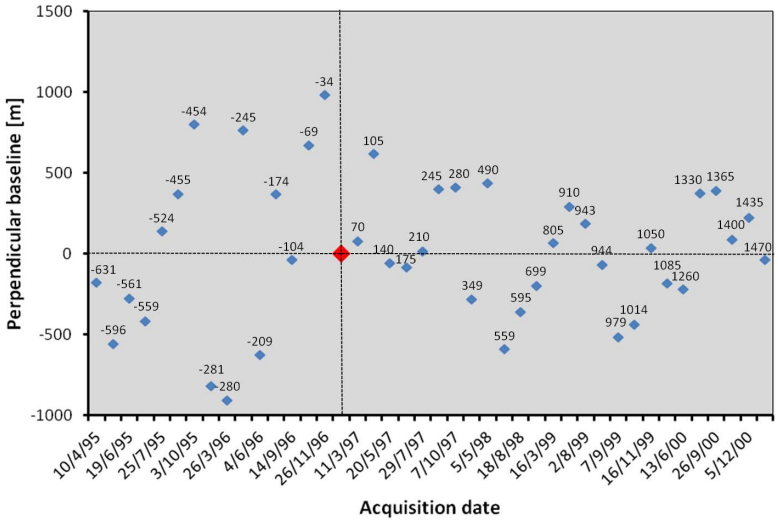

Fig. 3. Perpendicular baseline for each SAR scene of the PSI dataset, labeled with the temporal baseline. Parameters are referred to the master image which is indicated with the red square.

Fig. 4. Examples of the georeferencing accuracy of the WAP dataset: Thessaloniki breakwater (left) and Thessaloniki commercial harbour pier (right).

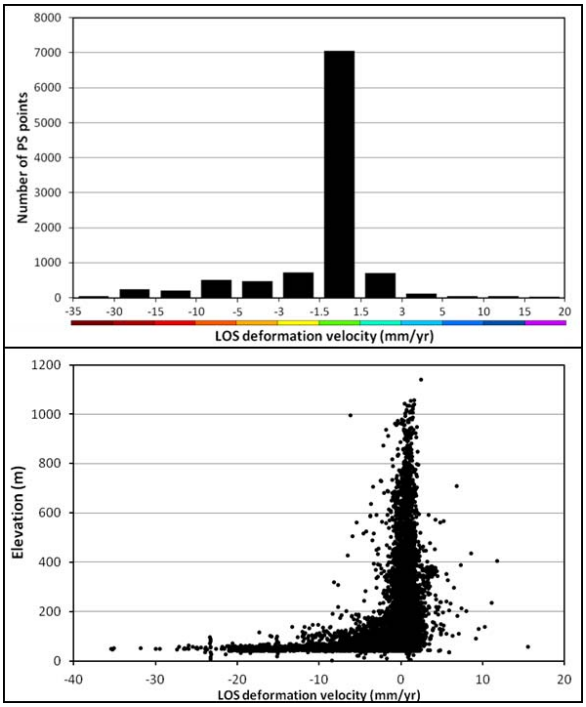

Fig. 5. Histogram of LOS deformation velocities distribution in the Anthemountas basin (above). Comparison between LOS deformation velocities with relative elevation for the dataset of PS points (below).

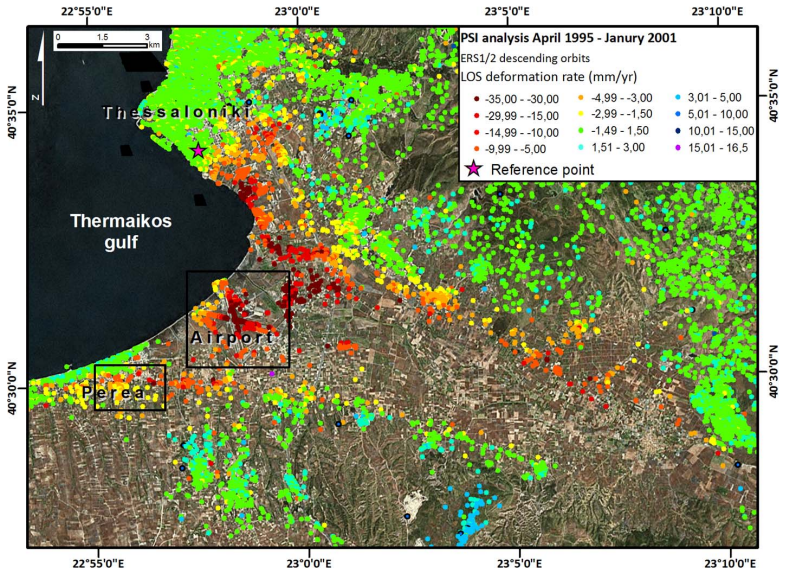

Fig. 6. LOS deformation rates in the Anthemountas basin. PSI map is overlaid on Visual Earth imagery. Adopted classification reflects the classes of the histogram of Fig. 5.

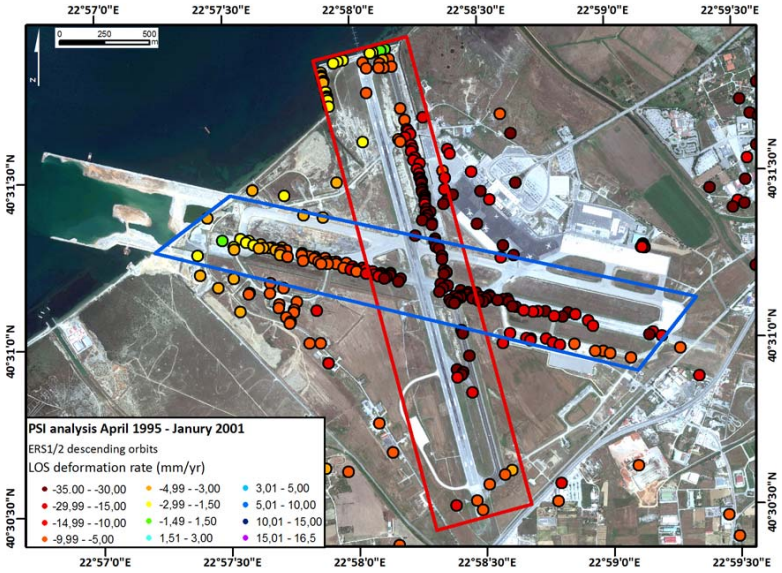

Fig. 7. LOS velocity map along the runway areas of "Macedonia" Airport. PSs inside the buffer zones have been extracted and analyzed to evaluate differential settlement.

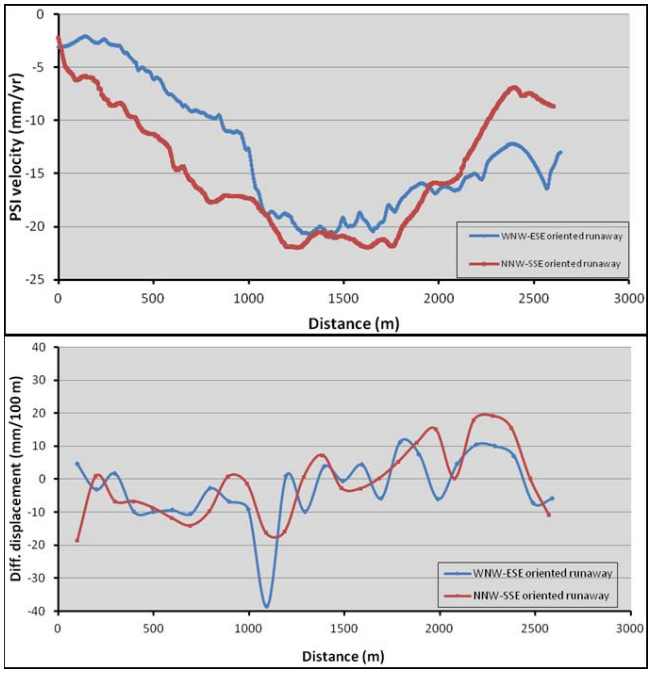

Fig. 8. Vertical deformation (Vv) of the LOS velocities measured along the runway areas of the Thessaloniki airport (above). Differential displacement along the runways area (below). Origin is set on the coastline.

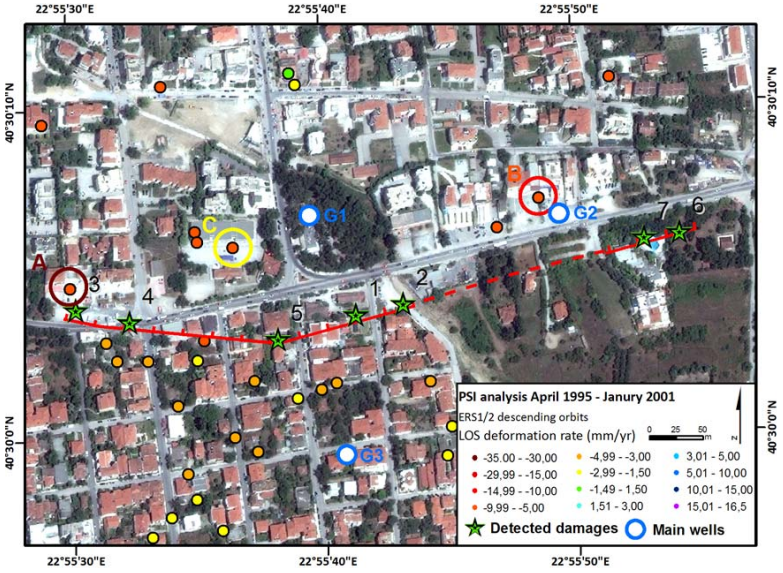

Fig. 9. Close-up of PSI data for Perea village. Green stars indicate surveyed points of Fig. 11.

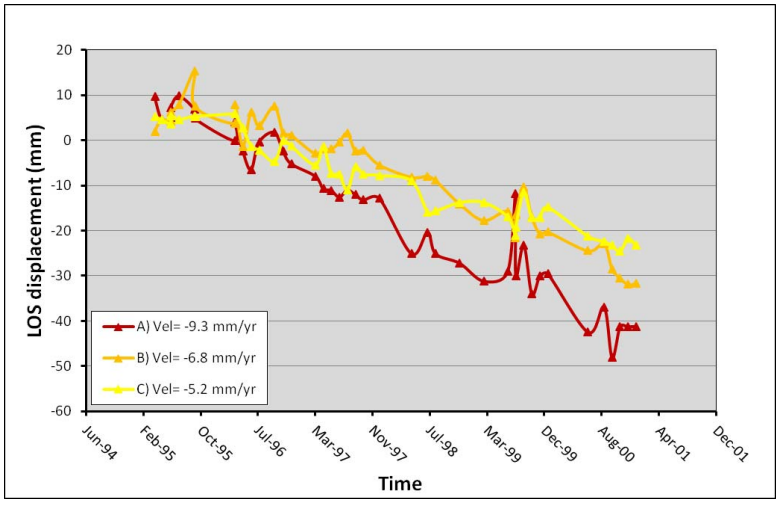

Fig. 10. Displacement time series and yearly velocities of PS A, B, and C (Fig. 9), located close to the damaged area of Perea village.

Fig. 11. Field evidences of ground ruptures in Perea. Coordinates are in UTM WGS 84 (projected). Damages witnessed at buildings (points 1 and 2), streets pavement (points 3 and 4), light constructions (points 5 and 7) and natural terrain (point 6).

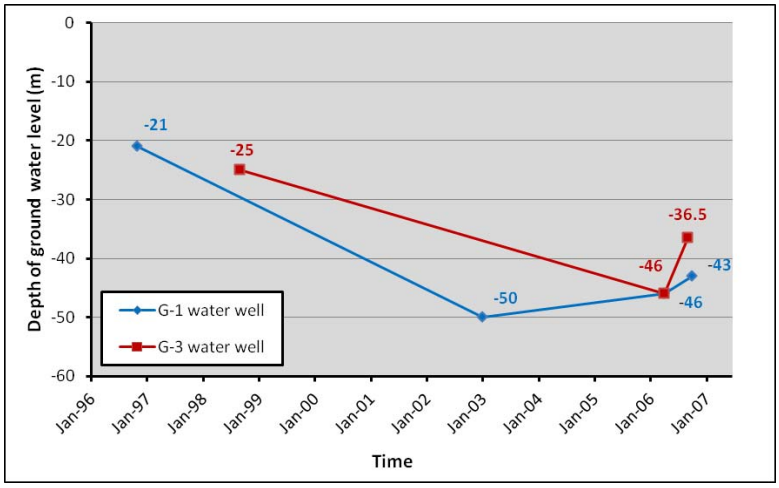

Fig. 12. Fluctuation of ground water table in G-1 and G-3 wells. Redrawn from Koumantakis et al. (2008).

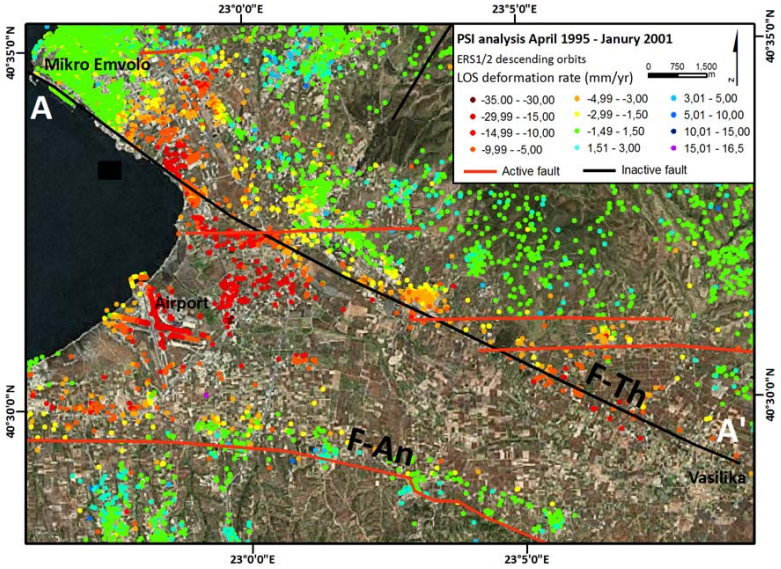

Fig. 13. Close-up of PSI data along the Thermi fault (F-Th).

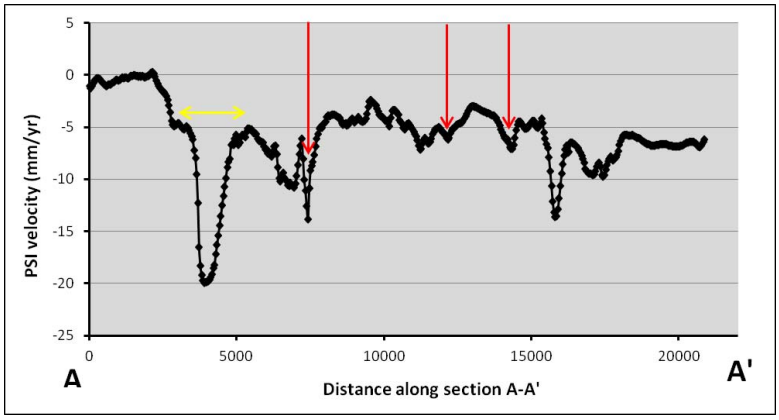

Fig. 14. LOS deformation rates measured along the profile coincident with the trace of the Thermi fault. The yellow arrow indicates the subsiding area close to the coastal zone. The red arrows indicate intersections between the Thermi fault and the three vertical active faults indicated in Fig. 13.